Virtual-crystal approach to aluminum-avoidance materials: A first-principles density-functional calculation of micas

Shigeru Suehara, Hirohisa Yamada, and Taizo Sasaki
National Institute for Materials Science, 1-1 Namiki, Tsukuba, Ibaraki 3050044, Japan
(Received 11 March 2012; revised manuscript received 19 May 2012; published 13 June 2012)

First-principles thermodynamic calculation of typical micas having a fractional occupancy of Al at the tetrahedral site is presented within a picture of the density-functional (perturbation) theory. A total-energy comparison conducted among the full set calculations on the Al tetrahedral site configurations within a mica unit cell confirmed an "aluminum-avoidance" rule. The energy difference of these structures is within room temperature energy of atoms. Therefore, it is most likely that the Al sites cannot be ordered in an ambient condition. A virtual atom generated by an average of Si (0.75) and Al (0.25) yields reasonable averaged features from the perspectives of its atomic eigenenergy and the optimized mica structures. The calculated infrared vibrational spectra with partial phonon density of states exhibit a marked difference between the Al-site specific and virtual-crystal models. However, the calculated thermodynamic properties for both models such as entropy and heat capacity exhibit good agreement with experimental values. An example of the virtual-crystal approach to estimation of a Na-K ion exchange energy is also presented. Results show that the virtual-crystal model can work well for energetic properties of aluminum-avoidance materials.

DOI: 10.1103/PhysRevB.85.224203 PACS number(s): 91.60.Ki, 91.65.An, 02.70.−c, 63.20.dk

I. INTRODUCTION

Hydrous phyllosilicates including clay minerals are the principal components of soils and key substances in both earth science and earth-friendly technologies.[1–3] Most of them can be categorized into two-dimensional aluminosilicate crystals mainly consisting of TO_4 (T = Si, Al, Fe,. . .) tetrahedra sheet and MO_6 (M = Mg, Al, Fe,. . .) octahedra sheets. These sheets can have widely various negative charges by substitution of T-site and/or M-site cations with atoms of different valence. Consequently, they form a stacking structure with an interlayer of counterions (K^+, Na^+,. . .) with or without water molecules. The most typical one can be found in the mica structure, which consists of T = Si with a small amount of T = Al (i.e., $T = Si_{0.75}Al_{0.25}$), M = Mg, and the interlayer K^+ cation. For such materials, it has been widely believed that an "aluminum-avoidance" rule based on the Pauling electrostatic valence rule governs the Al-site configuration among T sites.[4] In general, it is difficult to specify the Al atom positions in the aluminosilicate sheet. The Al (and Si) atoms are not well-ordered within the T sites in the crystal; namely, these materials have some structural ambiguity and can be interpreted to form a partially disordered system. Therefore, the results of the structural analyses are confined to showing that all T sites can be occupied by Al (and Si) with the probability expressed by its site occupancy.

Figure 1 portrays a mica (phlogopite) structure that is an ideal clay mineral. In this structure, the negative sheet charge originates from Al atoms at T sites with a ratio of 1/3 = Al/Si, and the interlayer K^+ ion can be understood to compensate the sheet charge.

Over the years, many studies have been undertaken to reveal the key factors to properties of these materials,[5–10] with control of both the sheet charge and interlayer ions (or charged molecules), producing a wide variety of structures and providing unique properties such as swelling and ion-exchange, etc., and functions for humidity control, catalytic, and water-protecting, etc., with environmental friendliness, which are not accessible in usual materials. However, theoretical studies of these materials have been deterred by the difficulty posed by their structural ambiguity. That is to say, the Al atom position cannot be specified in the periodic system.

To address this issue, we first performed first-principles density-functional theoretical (DFT) calculations on all possible structures with respect to the Al configuration within the mica model and verified the "aluminum-avoidance" rule.[11,12] Then, a virtual-crystal approach was assessed for use with this system to simplify its theoretical model.[13–15] Secondly, the density-functional perturbation theory (DFPT)[16] has been used to obtain the finite-temperature thermodynamic properties, which is expected to be important for developing practical products.

As described in this paper, the aluminum-avoidance rule is discussed through the analyses of energies, unit-cell volumes, and distances between the Al atoms. Examinations of the virtual-crystal model are conducted for entropies and heat capacities with infrared (IR) vibrational spectra and partial phonon densities of states. Finally, we present application examples of the virtual-crystal approach to other types of micas, such as muscovite, paragonite, and aspidolite, and estimate the Na-K ion-exchange energy of interlayer cations.

II. CALCULATION METHOD

Figure 1 portrays a schematic illustration of a typical mica, i.e., phlogopite ($KMg_3(OH)_2[T_4O_{10}]$) crystal structure consisting of a MgO_6 octahedral sheet sandwiched by TO_4 (T = Si,Al) tetrahedral sheets and cation (K) interlayer in a monoclinic cell (hereinafter, a 1*M* structure). The structure comprising two tetrahedral and one octahedral sheet is often designated as the "2 : 1" structure. For this study, we assumed $Si_{0.75}Al_{0.25}$ for the T site. Two formula units (f.u.), 44 atoms, and eight T sites (T_1–T_8) are found in the unit cell.[17] We used calculation models in which two of these T sites are

 ©2012 American Physical Society

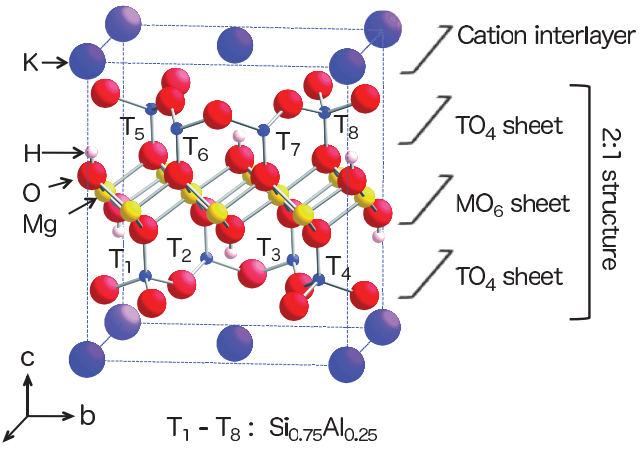

FIG. 1. (Color online) Schematic illustration of a monoclinic ($C2/m$) $1M$-mica structure, phlogopite, $KMg_3(OH)_2[T_4O_{10}]$. The experiment[17] has shown that T_1–T_8 sites are occupied by Si or Al with a ratio of Al/Si = 1/3 and lattice constants are of $a = 531.6$ pm, $b = 920.4$ pm, $c = 1031.0$ pm, and $\beta = 99.9°$. A sandwich structure of TO_4-MO_6-TO_4 is commonly designated as a "2 : 1" structure.

occupied by Al and the others by Si. Because we adopted the C_2 symmetry along the b axis for the initial structure, the full set of possible models includes 22 different structures.

For this study, the state-of-the-art QUANTUM-ESPRESSO[18] code based on the first-principles DFT and DFPT was used for the structural optimizations and phonon calculations. The exchange-correlation energy was approximated using the Perdew-Burke-Ernzerhof functional.[19] With the soft norm-conserving Troullier-Martins (TM) – type pseudopotentials of H, O, Na, Mg, Al, Si, and K provided by the FHI98PP site,[20] the plane wave energy cutoff (ecut) larger than 90 Ry and 2×1^2 Monkhorst-Pack (MP) k-point sampling were confirmed to be sufficient to obtain total energy difference of less than 1 mRy/atom from the calculations up to the ecut of 300 Ry for a most stable phlogopite model (i.e., the structure model with the Al atoms at T_1 and T_7 sites).[21] A convergence threshold of 10^{-10} Ry/atom was used for an electronic ground-state self-consistency error. The structure optimizations with no symmetry assumption were performed respectively to be residual stress and forces of less than 0.5 kbar and 0.1 mRy/bohr.

The calculation of the phonon at the Γ-point followed obtaining the equilibrium atomic positions. In brief, within the DFPT picture, the second-order derivatives of the energy, i.e., Hessian matrix determining the harmonic phonon frequencies of the system, are directly obtained by the electron-density linear response that can be self-consistently solved together with the first-order variations of both the Kohn-Sham orbitals and the self-consistent potential.[16] A convergence threshold of 10^{-14} was employed for the self-consistency error of the first-order potential variation. The sum rules[18,22] that guarantee translational symmetry and the charge neutrality for the system were imposed so that the energies of the acoustic phonon modes at the Γ-point (i.e., the lowest three energy modes) and the sum of the Born effective charges for all atoms vanished. A typical error of less than 1 cm^{-1} for the present vibrational frequency was estimated from the comparison between the phonon calculations of the 2×1^2 and 4×2^2 k-point meshes. The IR vibrational spectra were derived from the square of the dipole moment estimated by the sum of the product of the Born effective charge and the normalized vibrational eigenvectors at Γ point.[18,23]

TABLE I. Virtual atom (T_v) generation based on an average of 0.75-Si and 0.25-Al. Cutoff radius r_c (bohr), occupancy of electrons, eigenvalues (eV) for valence electrons for each channel l, and atomic mass for the T-site atoms, Al, Si, and T_v.

			Eigenvalue		
l	r_c	Occ.	AE	PS	Mass
T_v					27.8095
s	1.778	2.00	−10.040 832	−10.040 880	
p	1.960	1.75	−3.734 913	−3.734 903	
Al					26.9815
s	1.791	2.00	−7.752 965	−7.752 978	
p	1.974	1.00	−2.712 123	−2.712 100	
Si					28.0855
s	1.704	2.00	−10.812 915	−10.812 969	
p	1.879	2.00	−4.081 239	−4.081 228	

The pseudopotential (T_v) for the virtual atom at the T site was generated using the method of Fuchs *et al.* with the pseudonucleus charge Z^{PS} of 3.75 and the electronic configuration of $2s^2 2p^{1.75}$ as the average of 0.75-Si ($Z^{PS} = 4$) and 0.25-Al ($Z^{PS} = 3$).[24] Table I shows the generation condition, estimated atomic eigenvalues, and the atomic mass for the T_v atom compared with those of Al and Si atoms. Typical means used to obtain a virtual atomic pseudopotential have been presented by Ramer and Rappe, who pointed out the significance of the averaged eigenvalue defined by the average of the eigenvalues of the atoms to be mixed.[15] As shown in Table I, the eigenvalues for each channel by the generated T_v pseudopotential yield the averaged eigenvalues of Si (0.75) and Al (0.25). In the virtual-crystal model calculation, the T_v pseudopotential was used for all T sites, and the other calculation conditions such as ecut and k-point sampling were the same as those described above.

In Na-K ion-exchange calculations, as a virtual-crystal application example, we consider two systems: Na-micas in a KCl solid salt and K-micas in a NaCl one. As a countermica of phlogopite (K-mica), aspidolite ($NaMg_3(OH)_2[T_4O_{10}]$, 2 f.u. in a $1M$ unit cell[25]), known as Na-phlogopite, was used. We can compare the Helmholtz free energies of these systems directly and discuss the Na-K ion-exchange energy because the total composition is the same for each system of phlogopite with NaCl and aspidolite with KCl. Additionally, we examine the Na-K ion exchange energy for another type of mica with larger unit cells, namely, muscovite ($KAl_2(OH)_2[T_4O_{10}]$, 4 f.u., 84 atoms in a $2M$ unit cell[26]) and paragonite ($NaAl_2(OH)_2[T_4O_{10}]$, 4 f.u., 84 atoms in a $2M$ unit cell[27]). These $2M$ micas have a similar structure to that of phlogopite, but the stacking periodicity along the c axis is doubled and the octahedral sheets consist of AlO_6 instead of MgO_6 with one vacant M site.

Thermodynamic quantities such as entropy S and constant-volume heat capacity C_v were estimated within a harmonic approximation, i.e., these values were derived by differentiating

the Helmholtz energy function F:

$$F(T) = E + F^{\mathrm{ph}}(T),$$
$$F^{\mathrm{ph}}(T) = k_B T \sum_s \ln\left(2 \sinh \frac{\hbar\omega_s}{2k_B T}\right),$$

where E and F^{ph} respectively represent the electronic ground-state total energy and the phonon free energy function including the zero-point energy, with a given temperature T.[28] $\hbar$, k_B, and ω_s respectively denote Planck and Boltzmann constants, and phonon frequencies of mode s. Because the thermodynamic relationship gives $C_{\mathrm{v}} = -T(\frac{\partial^2 F}{\partial T^2})_V$ and $S = -(\frac{\partial F}{\partial T})_V$, we use the following equations for the thermodynamic properties:

$$C_{\mathrm{v}} = k_B \sum_s \left(\frac{\hbar\omega_s}{2k_B T}\right)^2 \sinh^{-2} \frac{\hbar\omega_s}{2k_B T},$$
$$S = k_B \sum_s \left[\frac{\hbar\omega_s}{2k_B T} \coth \frac{\hbar\omega_s}{2k_B T} - \ln\left(2 \sinh \frac{\hbar\omega_s}{2k_B T}\right)\right].$$

III. RESULTS AND DISCUSSION

Table II lists the relative total energy to the energy of the most stable structure and the volume of each unit-cell structure model St ij, in which T_i and T_j sites (see Fig. 1) are occupied by Al. The results of virtual-crystal approximation are also displayed. In this study, we assume that each unit cell model of phlogopite contains the same number of Al atoms, i.e., 2 Als/cell, because no report in the literature has described Al clustering. The calculation result has shown that the St17 model is the most stable. Table III shows the optimized structures of the St17 and virtual-crystal models, compared with the experimental values.

In Table II, it is noteworthy that the group with a relative energy higher than 10 mRy/cell (group 1) has two Al atoms in the same TO_4 sheet and the lower energy group (group 2) has one Al atom in each TO_4 sheet. Moreover, four of the highest energy structures in group 1 include $-AlO_4-AlO_4-$ tetrahedron chain with a Al-Al distance of ca. 310 pm, whereas the others exhibit a slightly lower energy with the $-AlO_4-SiO_4-AlO_4-$ chains. In group 2, the subgroup with d_{Al} larger than approximately 530 pm is found to exhibit the lower energy. Furthermore, the smaller volume structure appears to have the lower energy. This tendency is expected to reflect that the longer Al-Al distance and the smaller unit cell conditions stabilize the phlogopite more. The former condition coincides with the aluminum-avoidance rule.[4] An energy difference between the most stable phase and the most unstable one (i.e., St12 model) is found to be of ca. 26 meV/atom. It can be compared with the thermal energy of an atom at room temperature. It is therefore most likely that the Al site cannot be ordered in phlogopite, although the phlogopite crystal is expected to follow the aluminum-avoidance rule as shown in Table II.

TABLE II. Relative total energy (ΔE_{tot}) to that energy of the most stable model and volume (V) of the 1M-phlogopite unit-cell model Stij with Al occupying T_i and T_j sites are listed. Minimum distances between Al atoms (d_{Al}) and T_i and T_j sites (d_{ij}) are also displayed. Those of the virtual crystal (VC) are listed at the bottom.

Index ij for Stij model	ΔE_{tot} (Ry/cell)	V (10^8 pm^3)	d_{Al} (10^2 pm)	d_{ij} (10^2 pm)
Group 1[a]				
12 (34)	+0.084	5.179	3.05	3.05
14 (23)	+0.045	5.146	3.10	3.10
13 (24)	+0.030	5.145	5.33	5.33
Group 2[b]				
15 (26, 37, 48)	+0.002	5.164	4.92	4.92
16 (25, 38, 47)	+0.001	5.158	5.34	5.60
18 (27, 36, 45)	+0.001	5.049	5.32	5.67
17 (28, 35, 46)	0	5.047	5.32	7.10
VC	+1.014	5.031		

[a]Al atoms exist in the same TO_4 sheet.
[b]Each TO_4 sheet contains one Al atom.

TABLE III. Calculated phlogopite structures for the most stable St17 and virtual-crystal (VC) models with the experimental data (Ref. 17). Deviation from the experiment is shown in parentheses as a percentage.

	Calc. (St17)		Calc. (VC)		Expt.
Average bond length (10^2 pm)					
⟨Si-O⟩	1.644	(−0.8)			
⟨Al-O⟩	1.768	(+6.6)			
⟨T_{v}-O⟩			1.670	(+0.7)	1.658
⟨Mg-O⟩	2.081	(+0.4)	2.079	(+0.3)	2.073
⟨K-O_{inner}⟩	2.944	(−1.0)	2.953	(−0.7)	2.973
⟨K-O_{outer}⟩	3.458	(+2.0)	3.433	(+1.3)	3.389
⟨O-H⟩	0.959	(+17.0)	0.957	(+16.6)	0.820
Lattice constants (10^2 pm) and volume (10^8 pm^3)					
a	5.318	(+0.0)	5.322	(+0.1)	5.316
b	9.214	(+1.1)	9.202	(−0.0)	9.204
c	10.454	(+1.4)	10.423	(+1.1)	10.310
β	99.9	(+0.0)	99.7	(−0.2)	99.9
Volume	5.047	(+1.6)	5.031	(+1.3)	4.969

Although the virtual crystal exhibits the highest relative energy of +1.014 Ry/cell among the mica structures shown in Table II, its lattice constants and bond lengths listed in Table III reproduce the experimental values well. The O–H distance is observed as 95.8 pm in H_2O close to the calculated O–H distance in the mica despite the large discrepancy in the table. The experimental value[17] seems somehow much smaller than a typical O–H bond length. Increasing the total energy for the virtual crystal is expected to originate from averaging the repulsive Al-Al interaction by the T_{v} substitution for Al.

Figure 2 shows calculated entropies S and constant-volume heat capacities C_{v} of phlogopite compared with the available experimental values.[29] Both S and C_{v} reproduce the experimental data. No differences between St17 and virtual-crystal calculations were found, as shown in Fig. 2. Consequently, it can be noted that the virtual-crystal model in this study represents the overall phlogopite structural feature and basic thermodynamic properties, whereas the phonon frequencies show a qualitative difference between the Al-site specified and virtual-crystal models, as will be discussed in the following.

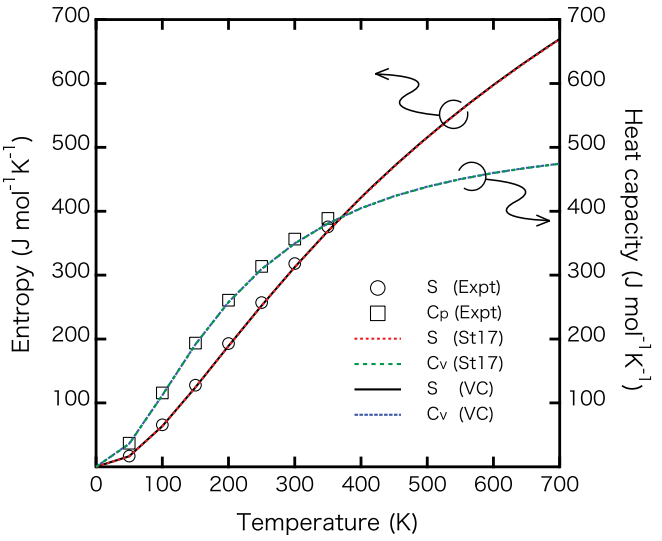

FIG. 2. (Color online) Calculated entropies (S) and constant-volume heat capacities (C_v) for the St17 and virtual-crystal (VC) models of phlogopite with the experimental plots referred from Ref. 29.

Figure 3 displays the experimental and theoretical IR vibrational spectra. The experimental spectrum of the natural phlogopite was traced from Ref. 30. Because the individual phonon mode is under the strong influence of local conditions, such as nuclear mass, chemical bonding, etc., the phonon spectrum of the virtual crystal is a reference system marking up the inhomogeneous system. The St17 model [Fig. 3(b)] reproduces the overall feature of the experimental IR spectrum [Fig. 3(a)] better than the virtual crystal [Fig. 3(c)], while a systematic redshift of the calculated spectra is somehow observed. In the range 650–1000 cm^{-1}, where Al–O and Si–O vibrations are expected from the IR experimentally obtained results,[30] a significant difference was found between St17 and virtual crystal models. For example, a peak below 800 cm^{-1} [Fig. 3(b)] denoted by the asterisk (*) disappears in the virtual crystal [Fig. 3(c)]. Moreover, the other peaks in this region in Fig. 3(b) are apparently reorganized as if they were merged to have an intense peak around 890 cm^{-1} in Fig. 3(c).

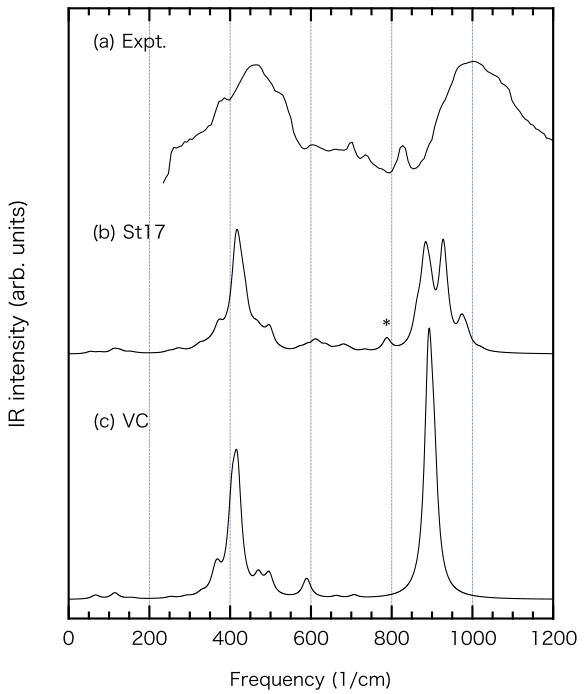

FIG. 3. (Color online) Infrared (IR) vibrational spectra for the phlogopite up to 1200 cm^{-1}. The experimental spectrum (a) for the natural phlogopite were traced from Ref. 30. The theoretical spectra for (b) St17 and (c) virtual-crystal (VC) models were obtained by a Lorentzian broadening of the calculated IR line spectra with a full width at half maximum (FWHM) of 24 cm^{-1}. The peak denoted by the asterisk (*) symbol originates mainly from the Al-O vibrations [see Fig. 4(a)] and corresponds to the Al-O peak at around 825 cm^{-1} in the experimental spectrum (a).

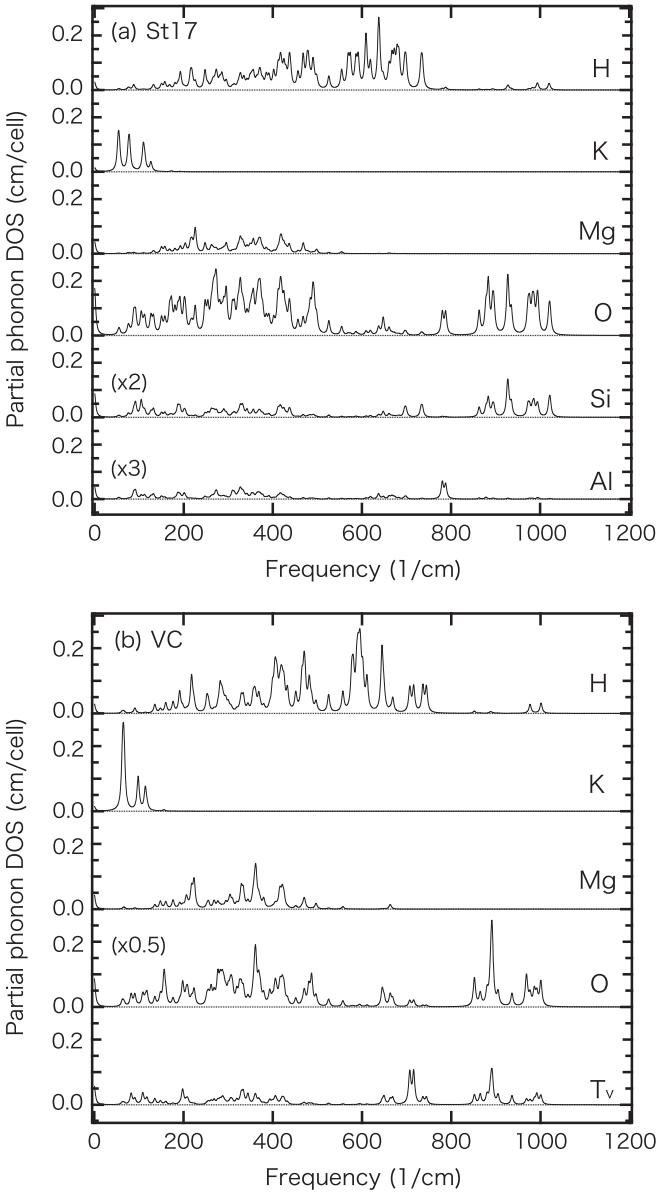

FIG. 4. Phonon partial density of states (DOS) for the (a) St17 and (b) virtual-crystal (VC) models. A Lorentzian broadening with a FWHM of 6 cm^{-1} is used to obtain the DOS from the line spectra of the phonon modes.

Partial phonon DOS (PDOS) in Fig. 4 reveals the origin of these IR peaks. The peak below 800 cm^{-1} denoted by asterisk in Fig. 3(b) can be assigned to the Al–O chemical bonds because of the large amplitude of the Al and O vibration in PDOS, as shown in Fig. 4(a). This is also consistent with the experimental interpretation of the peak around 825 cm^{-1} in Fig. 3(a).[30] In general, a chemical bond with lower atomic mass gives a higher frequency. However, the vibration frequencies for Si–O bonding appear to be higher than those of Al–O. This is expected to have originated from the bond length of Al–O that is greater than that of Si–O, implying that the Al–O bond is softer than the Si–O bond, as shown in Table III.

No significant difference was found between St17 and the virtual crystal for the PDOS of H, K, and Mg components [Figs. 4(a) and 4(b)]. The PDOS of T_v is not a simple average of PDOS for Si and Al. Consequently, the virtual-crystal approximation is apparently inappropriate to attack local-structure dependent problems, although the virtual-crystal approach is expected to be feasible to the thermodynamic properties based on these vibrational energies.

The systematic energy shift observed between the IR spectra of the experiment [Fig. 3(a)] and the theory [Fig. 3(b)] contrasts with the previous phonon studies,[16,23,31] where the experimental phonon dispersions are well reproduced without a significant phonon-energy shift. The origin of the shift in the present study seems open to question. The discrepancy might be slightly improved by the different calculation condition (e.g., different functional, pseudopotentials, number of energy sampling points, etc.). However, further consideration of this matter seems to be beyond the scope of this paper.

Finally, we show an application example of the virtual-crystal approximation to obtain the Na-K ion-exchange energy. Tables IV–VI summarize optimized lattice constants, thermodynamic properties of these materials, and ion-exchange energies with free energies, respectively. The same computing conditions have been applied to micas, and the denser MP mesh (12^3) was used for electronic energy integration and the phonon sampling for the salts.

As might be readily apparent in Tables IV and V, the virtual-crystal approximation for the micas works well with small deviations from the available experimental data in the structural and thermal properties. The free-energy difference of 5–9 kcal/mol between the Na-mica/KCl and K-mica/NaCl systems in Table VI indicates that a K-mica system is expected to be stabler than a Na-mica system in a salt environment. These ion-exchange energies are close to the values of 8–10 kcal/mol found through the thermodynamic analysis conducted by Zen.[36]

Consequently, the virtual-crystal approximation will yield some useful properties without time-consuming preliminary calculations for finding a proper site configuration of the T-site atoms. This approach is expected to work efficiently, especially for another aluminum-avoidance material with a different Al/Si ratio from the micas.

TABLE IV. Optimized virtual-crystal lattice parameters (a, b, c in 10^2 pm and β in degree) and calculation condition for each material. Deviations from the experimental data (Refs. 17 and 26–28) are shown in parentheses as a percentage.

	a	b	c	β
Mica species				
Phlogopite	5.322	9.202	10.423	99.7
	(+0.1)	(−0.0)	(+1.1)	(−0.2)
Aspidolite[a]	5.268	9.101	10.094	100.0
Muscovite	5.215	9.035	20.337	95.8
	(+1.1)	(+0.9)	(+1.3)	(+0.0)
Paragonite	5.162	8.937	19.518	93.6
	(+0.5)	(+0.4)	(+0.7)	(−1.0)
Salts				
NaCl[b]	5.647			
	(+0.1)			
KCl[b]	6.262			
	(−0.5)			

[a]Reference 25.
[b]A TM-type pseudopotential provided by FHI98PP was used for Na and Cl.[20]

TABLE V. Entropy and heat capacity at 298.15 K for micas by the virtual-crystal approximation with available experimental data (in J $mol^{-1}K^{-1}$) (Refs. 29 and 32–34). Deviations from the experimental data are shown in parentheses as a percentage.

Mica species		Entropy		Heat capacity	
Phlogopite	Calc.	310.40	(−1.7)	348.52	(−1.9)
	Expt.[a]	315.9		355.1	
Aspidolite[b]	Calc.	315.50		346.56	
Muscovite	Calc.	288.53	(−0.1)	321.29	(−1.4)
	Expt.[c]	288.70		325.99	
Paragonite	Calc.	284.38	(+2.6)	319.91	(−0.5)
	Expt.[d]	277.2		321.5	
NaCl	Calc.	74.91		48.05	(−5.4)
	Expt.[e]			50.79	
KCl	Calc.	80.43		48.39	(−6.0)
	Expt.[e]			51.46	

[a]Reference 29.
[b]No available experimental thermodynamic data.
[c]References 32 and 33.
[d]Reference 29.
[e]Reference 35.

TABLE VI. Free energy F (Ry/f.u.) and the Na-K ion-exchange energy ΔF[Na-mica,K-mica] = F[Na-mica] + F[KCl] − F[K-mica] − F[NaCl] (kcal/mol) at temperatures of 0 K and 298.15 K from virtual-crystal approximation.

	0 K[a]	298.15 K
Free energy (Ry/f.u.)		
Phlogopite	−425.181	−425.211
Aspidolite	−425.036	−425.068
Muscovite	−424.997	−425.026
Paragonite	−424.862	−424.890
NaCl	−31.161	−31.167
KCl	−31.278	−31.285
Na-K ion-exchange energy (kcal/mol)		
ΔF[Aspidolite, Phlogopite]	8.79	7.84
ΔF[Paragonite, Muscovite]	5.65	5.65

[a]Zero-point energies were considered.

IV. CONCLUSION

We have shown the first-principles calculations on the typical micas having a fractional occupancy of Si and Al at the tetrahedral site within a picture of the density-functional (perturbation) theory and the harmonic approximation. The total energy comparison among the full set calculations on the Al tetrahedral site configurations within a 1*M* mica unit cell confirmed an aluminum-avoidance rule. The energy difference of these structures is within room temperature energy of atoms. Therefore, it is most likely that the Al sites cannot be ordered in an ambient condition. A virtual atom for the virtual-crystal model was generated from the averaged nucleus charge of Si (0.75) and Al (0.25) and it yields reasonable averaged features in the views of its atomic eigenenergy and the optimized mica structures. The calculated infrared vibrational spectra with partial phonon density of states exhibit a marked difference between the Al-site specific and virtual-crystal models. However, the calculated thermodynamic properties such as entropy and heat capacity for the typical micas exhibited good agreement with the experimental values. An example of the virtual-crystal approach to estimating a Na-K ion exchange energy is also presented. For estimating total energetic properties of aluminum-avoidance materials, the virtual-crystal approximation is expected to work effectively.

ACKNOWLEDGMENTS

All calculations were performed using workstations (Xserve; Apple Computer Inc.) and a numerical materials simulator (SGI Co. Ltd.) at our institute (NIMS). One author (S.S.) wishes to thank Professor K. Kawamura (Okayama Univ., Japan), Dr. K. Tamura, and Dr. T. Echigo (NIMS) for fruitful discussions related to the aluminum-avoidance rule, Professor A. M. Rappe (Univ. Pennsylvania, USA), Dr. M. Arai (NIMS), and Dr. K. Kobayashi for helpful hinting for the virtual atomic potential generation, and Dr. T. Aizawa (NIMS) for critical comments related to the manuscript.

[1] F. Bergaya, B. K. G. Theng, and G. Lagaly, *Handbook of Clay Science* (Elsevier, Amsterdam, 2006).
[2] K. Morimoto, K. Tamura, N. Iyi, J. Ye, and H. Yamada, J. Phys. Chem. Solids **72**, 1037 (2011).
[3] H. Yamada, K. Tamura, Y. Watanabe, N. Iyi, and K. Morimoto, Sci. Technol. Adv. Mater. **12**, 064705 (2011).
[4] W. Lowenstein, Am. Mineral. **39**, 92 (1954).
[5] D. R. Collins and C. R. A. Catlow, Am. Mineral. **77**, 1172 (1992).
[6] E. J. Palin, M. T. Dove, M. D. Welch, and S. A. T. Redfern, Mineral. Mag. **69**, 1 (2005).
[7] H. Sakuma, T. Kondo, H. Nakao, K. Shiraki, and K. Kawamura, J. Phys. Chem. C **115**, 15959 (2011).
[8] K. Kawamura, Y. Ichikawa, M. Nakano, K. Kitayama, and H. Kawamura, Eng. Geology **54**, 75 (1999).
[9] E. S. Boek and M. Spirk, J. Phys. Chem. B **107**, 3251 (2003).
[10] C. I. Sainz-Diaz, V. Timon, V. Botella, E. Artacho, and A. Hernandez-Laguna, Am. Mineral. **87**, 958 (2002).
[11] P. Hohenberg and W. Kohn, Phys. Rev. **136**, B864 (1964).
[12] W. Kohn and L. J. Sham, Phys. Rev. **140**, A1133 (1965).
[13] L. Nordheim, Ann. Phys. (Leipzig) **9**, 607 (1931).
[14] T. Muto, Sci. Pap. Inst. Phys. Chem. Res. (Jpn.) **34**, 377 (1938).
[15] N. J. Ramer and A. M. Rappe, Phys. Rev. B **62**, 743R (2000).
[16] S. Baroni, S. de Gironcoli, A. D. Corso, and P. Giannozzi, Rev. Mod. Phys. **73**, 515 (2001).
[17] G. J. Redhammer and G. Roth, Am. Mineral. **87**, 1464 (2002).
[18] P. Giannozzi, S. Baroni, N. Bonini, M. Calandra, R. Car, C. Cavazzoni, D. Ceresoli, G. L. Chiarotti, M. Cococcioni, I. Dabo *et al.*, J. Phys.: Condens. Matter **21**, 395502 (2009), [http://www.quantum-espresso.org].
[19] J. P. Perdew, K. Burke, and M. Ernzerhof, Phys. Rev. Lett. **77**, 3865 (1996).
[20] M. Fuchs *et al.*, [http://www.fhi-berlin.mpg.de/th/fhi98md/fhi98PP/].
[21] H. J. Monkhorst and J. D. Pack, Phys. Rev. B **13**, 5188 (1976).
[22] X. Gonze and C. Lee, Phys. Rev. B **55**, 10355 (1997).
[23] P. Umari and A. Pasquarello, Diam. Relat. Mater. **14**, 1255 (2005).
[24] M. Fuchs and M. Scheffler, Comput. Phys. Commun. **119**, 67 (1999).
[25] A 1*M*-phlogopite model with substituting Na for the K interlayer cation was used for an aspidolite structure.
[26] S. Guggenheim, Y. H. Chang, and A. F. K. van Groos, Am. Mineral. **72**, 537 (1987).
[27] P. Comodi and P. F. Zanazzi, Phys. Chem. Mineral. **24**, 27 (1997).
[28] C. Kittel, *Introduction to Solid State Physics* (John Wiley & Sons, Inc., New York, 1986).
[29] R. A. Robie and B. S. Hemingway, Am. Mineral. **69**, 858 (1984).
[30] D. M. Jenkins, Phys. Chem. Miner. **16**, 408 (1989).
[31] S. Suehara, T. Aizawa, and T. Sasaki, Phys. Rev. B **81**, 085423 (2010).
[32] L. P. Ogorodova, L. B. Melchakova, and I. A. Kiseleva, Electronic Sci Info. J.: Herald of the Department of Earth Sciences RAS **21** (2003) [http://geo.com.ru/conf/khitariada/1-2003/informbul-1_2003/mineral-7e.pdf].
[33] N. D. Chatterjee and W. Johannes, Contr. Mineral. Petrol. **48**, 89 (1974).
[34] N. D. Chatterjee, Contr. Mineral. Petrol. **27**, 244 (1970).
[35] F. H. Ree and A. C. Holt, Phys. Rev. B **8**, 826 (1973).
[36] E.-A. Zen, Am. Mineral. **57**, 524 (1972).